Biochemical response of human endothelial and fibroblast cells to silver nanoparticles

Cristofher Victor Vivas Palomares
  Instituto de Física da USP

Jennifer Adriane Santos
  Instituto de Física da USP

Yan Borges Barreto
  Instituto de Física da USP

Sergio Hiroshi Toma
  Instituto de Química da USP

Jonnatan Julival Santos
  Instituto de Química da USP

Marco Antonio Stephano
  Faculdade de Ciências Farmaceuticas da USP

Cristiano Luis Pinto Oliveira
  Instituto de Física da USP

Koiti Araki
  Instituto de Química da USP

Adriano Mesquita Alencar
  Instituto de Física da USP

Antonio Carlos Bloise (✉ acbloise@if.usp.br)
  Instituto de Física da USP

Article

Abstract

Nowadays the bactericidal and antimicrobial properties of silver nanoparticles, AgNPs, in addition to their cytotoxic effects, have been explored to properly modulate cell biochemistry processes in order to improve the healing of wounds. Herein we investigate the cytotoxicity and metabolic profiling of two human cell lineages, the fibroblast FN1 and endothelial HUV-EC-C, planning doses of AgNPs and incubation times. Cytotoxicity assays showed consistent decrease in proliferation rates, viable cells number, and average surface areas. Metabolomics based on proton Nuclear Magnetic Resonance was successfully used to obtain quantitative and qualitative changes in metabolic events triggered by silver treatments. The metabolic profiling provided by endo- and exometabolome revealed biochemical changes induced on treated cells compared to controls. Glycolytic pathway is up-regulated due to the elevation in glucose consumption; however, the consequent elevation in pyruvate production seems to be wasted by cells to generate energy by aerobic means that are choosing to oxidize it to acetate. Aminoacid metabolism is down-regulated, signalizing the protein degradation mechanism. Tricarboxylic Acid Cycle is also down-regulated, indicating a starvation situation once succinate was left over in the culture media. Concurrently, the ketogenic pathway is up-regulated due to the excess of acetone. Changes in pyroglutamate metabolism were detected indicating the up-regulation of glutathione biosynthesis used to equilibrate the effects induced by oxidative stress, in accordance with the N-Acetylcysteine finds. Phospholipid metabolism is down-regulated, as revealed by the changes in O-Phosphocholine and Sn-Glycerol-3-PC levels, signaling reduction in the cellular proliferation rates. To the best of our knowledge, this is the first report describing AgNP-induced changes in the UDP-GlcNAc levels, which plays an essential role in modifying nucleocytoplasmic proteins. In summary, AgNPs can induce oxidative stress and cytotoxicity in endothelial and fibroblast cells, influencing their endo- and exometabolome.

Introduction

Silver has been used since ancient times to heal skin wounds. Much has been discovered in the past fifteen years about the bactericidal and antimicrobial properties of silver nanoparticles (AgNPs), the most primarily commercialized nanomaterial due to its antiseptic and disinfectant properties. Silver nanoparticles are used to produce antifungal, antibacterial, and antiviral products [1-3], including coatings for surgical instruments and cutaneous wounds [4,5]. Studies *in vivo* have confirmed faster healing by the application of AgNPs on skin wounds in models in mice [6]. Despite their beneficial properties, serious toxicological effects have also been reported in several *in vitro* and *in vivo* model systems [7]. Although AgNPs exhibit low acute toxicity *in vivo*, systematic accumulation in tissues and organs could lead to chronic toxicity [8]. Systematic *in vitro* studies demonstrated some adverse effects in different types of cells, including glioblastoma [9] and mesenchymal stem cells [10] and platelets [11]. However, few studies focus on cells involved in tissue repairs, such as microvascular endothelial cells, fibroblasts, and macrophages. Exposure of SVEC4-10 line murine endothelial cells to AgNPs significantly increased angiogenesis and activated Vascular Endothelial Growth Factor (VEGF) [12]. In contrast, AgNPs inhibited VEGF-induced cell proliferation in bovine retinal endothelial cells [13] and exhibited significant cytotoxicity

on brain endothelial cells [14]. Cytotoxic effects on mouse embryo fibroblast cells were reported by Arora *et al.* [15], where a decrease in mitochondrial function and increased levels of reactive oxygen species (ROS) also have been observed *in vitro*. On the other hand, Rigo *et al.* [16] confirmed that AgNPs impair the mitochondrial function in dermal fibroblasts, but not to an extent enough to promote cell death. Also, studies demonstrated that AgNPs induce solid oxidative stress on TPH-1-derived human and alveolar macrophages [17,18], reinforcing the most commonly used model to explain the *in vitro* toxicity of AgNPs [19].

As shown above, there seems to be a consensus on the nanotoxicity of AgNPs, but the discrepancies among the studies are still relatively high, presenting low reproducibility. Several reasons can be offered to account for this, such as the high degree of phenotype heterogeneity of the different model cells, significant differences in biodistribution and cellular uptake, and intracellular traffic and distribution. Accordingly, the toxicity is assumed to depend on physical properties such as size, shape, composition, and state of aggregation [20], which can strongly affect biological responses [20]. For this reason, the nanotoxicological behaviors present subtle differences between them, making direct comparisons inappropriate unless in the case of nanomaterials with a similar well-defined structure, composition, and surface chemistry.

In this work we demonstrate the inherent cytotoxicity of AgNPs and its impact on cellular growth and associated metabolic events, as described in specific metabolic pathways, as well as its possible manipulation to control the rate of cellular events triggered during the wound healing process. For this purpose, a systematic study was carried out based on standard cytotoxic assays and metabolomics using magnetic resonance spectroscopy of human cells undergoing dose- and time-dependent treatments employing a silver nanoparticle previously characterized by dynamic light scattering, zeta-potential, ICP-OES, and small-angle x-ray scattering (Supplementary Information) to demonstrate its physicochemical properties.

Results

In this work, we conducted standard cytotoxic assays and metabolomics in two lineages of cells, FN1 and HUV-EC-C, used as models to study wound healing induced by silver nanoparticles. The cells were exposed to a planned set of doses of AgNP during defined incubation times, and the effect on the average cellular growth and cytotoxicity was evaluated. Based on these first exploratory assays, relevant information on the intervals of AgNPs molar concentrations and incubation times were obtained and used to design the set of optimized conditions for the magnetic resonance experiments to study the main metabolic changes triggered by the nanoparticles treatment on each lineage. For such a purpose, both the cellular extracts and culture medium were evaluated in order to provide the fullfill metabolic profiling of cells summarized by the endometabolome and exometabolome, respectively [21]. The first one provides a direct evaluation of the cellular metabolic status until methanol addition interrupts cell metabolism, lysis, and extraction of the metabolic components for analysis, which was performed by monitoring the levels

of endogenous metabolites. The analyses of culture media components, such as aminoacids and some vitamins that were exogenously consumed by cells, in addition to regular and treated cell metabolites that were excreted, can be used to access indirectly the cellular metabolic status. The endometabolome and exometabolome analysis provide the most comprehensive and complete perspective about the metabolic scenery of cells exposed to silver nanoparticles and can reveal interrelated processes in the same metabolic pathway. Furthermore, it tells us about exclusive characteristics of a determinate kind of sample, for instance, the phospholipid composition of the cellular membrane [22].

Silver nanoparticles. The effect of silver nanoparticles depends on their interaction and uptake by cells, which depend on parameters such as shape, size, and surface potential of citric acid stabilized AgNP stock dispersion. This last parameter tends to be sensitive to ionic strength and agglomerate in higher ionic strength aqueous biological media. Also, its protecting molecular layer is weakly bound on nanoparticle surfaces. It tends to be easily replaced by molecules that can bind more strongly, commonly present in the culture medium, such as peptides and proteins, phosphate, and other components. Accordingly, experiments were conducted to evaluate the colloidal stability of nanoparticles in our control medium (DMEM culture medium supplemented with 10% v/v of FBS) necessary to support cellular metabolism during incubation. However, no significant change was observed by DLS.

Cytotoxicity assays. The CGK results summarized in Fig. 1 were organized by concentrations shown in separate panels, each containing the lineages differentiated by symbols, red circles, and green squares, to optimize the presentation of results. Analyzing these panels, we can first glimpse the impact of AgNP on the cellular viability by the impact on their proliferation rates [23]. As can be confirmed in Fig. 1, both FN1 and HUV-EC-C lineages present a similar proliferation behavior up to 48 hours in the absence of AgNP, followed by an apparent reduction in the cell population that can be associated with the depletion of culture medium nutrients and the natural process of cellular death by competition for space. Also, it is possible to see by analyzing the data in that range that FN1 is more sensitive to the presence of silver nanoparticles, and the proliferation is more strongly impacted. Such a tendency can be qualitatively monitored by the average time-dependent curves estimated from the linear fits of the rates of expansion ($\tau > 0$) and reduction ($\tau < 0$) of cells populations incubated as a function of the silver molar concentration, thus separating the effects of natural cell death from that induced by AgNP cytotoxicity and defining the rates at which these phenomena occur.

When nanoparticles are added, the cytotoxic response exhibited by FN1 and HUV-EC-C for the first 48 hours, where the cell number should be naturally expanding, indicates a continuous decrease in the proliferation rates and an increasing tendency of cell death. As shown in Fig. 1, the cells from FN1 lineage present $|\tau| < 0$ at [AgNPs] as low as 25 μM, whereas HUV-EC-C showed similar $|\tau| < 0$ at [AgNP] of 50−75 μM, demonstrating much lower sensitivity to the cytotoxic effects of AgNP. As expected, for incubation times longer than 48 hours, the estimated values of τ are always negative for these two lineages suggesting a reduction in their respective populations by a combined effect of natural cell death and that induced by AgNP cytotoxicity. Furthermore, AgNPs showed pronounced cytotoxicity at concentrations

higher than 75 µM, mainly above 100 µM, where both FN1 and HUV-EC-C cells exhibited quite similar behavior.

In order to isolate the cytotoxic effects induced by AgNP and the impact on the cellular morphology of the two lineages, some conditions were assumed. First, the incubation time within which the control cells were proliferating should be considered mainly, i.e., from 0 to 24 hours and from 24 to 48 hours, where 0 hours is the moment after 12 hours of incubation for cell stabilization in the absence of silver nanoparticles. Each FN1 and HUV-EC-C cell was assumed to be disc-shaped. The average diameter of the disc was measured in the Neubauer chamber using a microscope and a scale considering up to 10 cells for statistics. Such measurement was carried out after incubation for 24 and 48 hours and different concentrations of silver nanoparticles. In the Figs. 2 and 1 of Supplementary Information are plotted the obtained values for the average surface areas of cells calculated from their diameters.

Silver nanoparticles are considered low toxicity materials, but the optical microscopy images shown in the upper panels of Fig. 2 after 24 and 48 hours of incubation reveal cellular detachment and the presence of apoptotic bodies, as well as a tendency to decrease the diameter and related surface area, indicating a significant impact on the normal cell metabolism. The intervals of concentrations in which these tendencies occur are different depending on the cell lineage, showing important and distinct cellular resiliency against cytotoxic effects, following the previous results obtained for CGK assays. Furthermore, on average, the surface area of cells tends to decrease as the concentration and time of AgNP treatment increases, as shown in Fig. 1b of the Supplementary Information.

Figure 2b,c present the main results for the Neubauer counter and MTT assays, respectively, as the plots of "Number of viable N_{cells} cells *vs.* [AgNP]" and "Absorbance at 570 nm *vs.* [AgNP]" for the FN1 and HUV-EC-C cell lineages investigated as a function of AgNP (silver) molar concentration and incubation times up to 48 h, corresponding to the phase at cellular expansion. The significant cytotoxicity of silver nanoparticles is apparent in all concentrations, especially for FN1 cells, which becomes more evident after 48 hours for the lowest doses (25 and 50 µM). The analyses of these plots provide the first demonstration of the combined dose-dependent cytotoxicity induced by AgNP that allowed us to define the low and high toxicity ranges, respectively, denominated sublethal and lethal doses, used to choose the appropriate range of concentrations to prepare the samples for magnetic resonance experiments. Nevertheless, the range of concentrations and incubation times in which they are observed are more or less well-defined and different depending on the cell lineage, reinforcing the premise that they present specific tolerances to the toxic effects of AgNP. For instance, in Fig. 2b, FN1 cells seem tolerant to [AgNP] doses up to 50 µM.

In comparison, a significant decrease in the cell population can be observed after 24 and 48 hours of incubation (8% and 36%) at concentrations equal to or higher than 50 µM, as compared to the control (0 µM). This behavior suggests the presence of dose- and time-dependent cytotoxic effects where the first concentration range can be considered sub-lethal doses. However, the [AgNP] dose of 75 µM induced a clear decrease in the cell population, respectively, of 56% and 63% after 24 and 48 hours, as compared to

control, which seems to be less dependent on incubation time. Accordingly, nanoparticle concentrations above 75 µM were assumed to be lethal to the FN1 cell lineage. In contrast, the ranges of sublethal and lethal doses for HUV-EC-C cells seem to be shifted to lower silver nanoparticle concentrations. For example, 50 µM of AgNP reduced the cell population by 17% and 47% after 24 and 48 hours, compared with control, which also defines this range as the sub-lethal. Similar to FN1 cells, an apparent decrease in the HUV-EC-C cell population of, respectively, 55% and 62% after 24 and 48 hours were observed upon incubation with 75 µM of AgNP and the dependence on the incubation time, such that concentrations higher than that were assigned as lethal. The MTT results, summarized in Fig. 2c, follow the tendencies observed in Fig. 2b, demonstrating a dose and incubation time-dependent cytotoxicity. However, the extension to which the effects are related to the cellular metabolic events is still an open problem in the literature. Below, we address this issue for the first time using the magnetic resonance spectroscopy technique.

Nuclear magnetic resonance and statistical analysis. Nuclear magnetic resonance spectroscopy is a powerful tool for characterizing molecular species. Each molecule has a spectral signature that can be used to identify them; if well-resolved enough, spectra can be obtained. This signature implies removing any contribution that can decrease the homogeneity of the applied main magnetic field and shimming procedure for each measurement. Cell extract and corresponding culture medium samples of cells after 24 and 48 hours of incubation with AgNP were measured to assess the changes in the endometabolome and exometabolome. The ^{1}H-NMR spectroscopy results obtained for the FN1 and HUV-EC-C cells exposed to four different AgNP concentrations and the control (no AgNP) are shown in Fig. 3 and Fig. 4, respectively.

Each metabolite has characteristic peaks in the spectrum, whose integrated area is proportional to the relative metabolite concentration or level. Even though most high-resolution lines have been successfully identified, no apparent differences can be observed directly in their corresponding intensities, as expected for changes in their concentrations induced by the treatment with AgNP. The metabolite level is more suitable for the multi- and univariate statistical methods to access the biochemical cell's response induced by the treatment with silver nanoparticles. The first step of the multivariate method is to identify the tendencies of clustering among groups of samples with similar metabolomes. This analysis was performed using supervised PLS-DA, and the results are shown in the scores plots shown in Fig. 5 and Fig. 6. The second step was analyzing the VIP scores and identifying the metabolites responsible for such tendencies [24].

Let us first look at the results for 24 hours of AgNP exposition. In Fig. 5a,b, one can notice in the scores plots that in the combination Comp. 1 *vs.* Comp. 2, clusters of points are ascribed to distinct groups in separated quadrants of Hotelling's ellipses with different distances among their respective distribution centers. For instance, the separation between the control groups and the groups treated with 50 µM of AgNP is larger than the distance between 75 and 100 µM. Furthermore, groups in the right quadrants are pretty separated from those in the left one. However, inspecting the combination Comp. 1 *vs.* Comp. 3 in Fig. 5c,d at the same incubation time, the previous scenery seems to be inverted, as can be seen in the

scores plots of both cell extracts and culture medium samples. Overall, the isolated contribution of each component of the generated model tends to decrease as the order of components increases [25,26]. The percentual values in the brackets of each component evidence that observation. Thus, the combination of the first two consecutive components, Comp. 1 *vs.* Comp. 2, is expected to have higher statistical differences in the system than the combination of the first with the third, Comp. 1 *vs.* Comp. 3, when the differences tend to decrease. This rule holds, and the combination Comp. 2 *vs.* Comp. 3 presents even fewer differences than the previous ones (not shown). Therefore, we can conclude that in the first case of combination Comp. 1 *vs.* Comp. 2 of the Fig. 5a,b, the variation in the levels of the metabolites is intense for the first dose of treatment, 50 μM, as compared with control, and tends to diminish for the higher doses, 75 and 100 μM. However, the 75 and 100 μM doses also keep differences in the levels of their respective metabolites but are lower in magnitude than the control and cells treated with 50 μM AgNPs. In summary, for 24 hours of treatment, the results obtained for cells and culture media indicated that most changes in FN1 metabolites occur in the first dose of treatment, decreasing for the higher ones, probably indicating a homeostatic response.

Now, we can look at the results after 48 hours of treatment with FN1 cells with AgNP. PLS scores can be interpreted using the same arguments presented previously. For instance, the combination of Comp. 1 *vs.* Comp. 2 in Fig. 5e suggests that the dose inducing higher modifications in metabolites levels is 25 μM rather than 50 μM used within 24 hours of treatment. However, if we inspect the same combination of components for culture media samples in Fig. 5f, the doses of 25 and 50 μM seem to be very similar, suggesting the induction of almost the same metabolomic effect on the cells, but that now can be detected indirectly in samples of culture media. The correlation between Comp. 1 *vs.* Comp. 3 at the same doses of 25 and 50 μM is now quite similar for cell extract (Fig. 5g) but more differentiated in the culture medium samples (Fig. 5h). Based on this behavior, we could argue that longer incubation times, 48 hours, and lower doses can impact the metabolism nearly in the same way as higher doses and shorter time of incubation, 24 hours. Similar changes were first detected in cell extracts and then in culture media of FN1 cells upon treatment with AgNP.

The PLS scores plots shown in Fig. 6a-h addressing cells from HUV-EC-C lineage reveal that genetic factor plays an essential role in the way cells metabolome respond to dose and incubation time with AgNP, as evidenced by the cytotoxic results. For instance, the combination Comp. 1 *vs.* Comp. 2 for 24 hours of treatment shows that the distribution centers of control groups and 50 μM are now close to each other, whereas 75 and 100 μM are more distant from the metabolome of cell extract samples (Fig. 6a). This situation changes for the culture medium samples and at the same time of exposition. The distributions of groups for cells treated with 50 and 75 μM are close to each other and more distinct from the control and 100 μM groups (Fig. 6b). Such a metabolic profile indicated that HUV-EC-C cells tend to be more resilient in changing the levels of their metabolites when treated with AgNP doses starting with 50 μM and 24 hours of incubation than the FN1 in the same experimental conditions. On the other hand, the proximity of the distribution centers of the 50 and 75 μM groups seems to indicate a different aspect of

cell metabolism that can be now accessed from the data from the culture medium samples (Fig. 6b) compared with data from the cell extract samples (Fig. 6a).

In general, when we used statistical multivariate methods such as PCA and PLS-DA, this last one the choosed to deal our data, we present the axis in the graphics as PCx vs. PCy (abbreviation for principal components) for PCA method and Comp.x vs. Comp.y (just components) for PLS-DA. There is a difference between the methods related with the statistic used in each one: variances for PCA and co-variances for PLS-DA. Indeed, PCA has zero covariances and maximizes variances organized in descend order, so receiving the name de principal components for the axis in the scores plots. The axis in scores plot of PLS-DA do not have this denomination because it is calculated in another mathematical way, receiving just the name "component". Anyway, it is hard to explain, but is a general way to describe the axis in PLS results. Besides, all graphics of scores plot were built in this way. We already published one paper and it was gone alright.

The information brought by the combination of Comp. 1 *vs.* Comp. 3 is complementary to that revealed by the combination of Comp. 1 *vs.* Comp. 2, corroborating that the metabolites levels of control and cell exposed to 50 µM of AgNP can exhibit only minor differences (Fig. 6c), that are also present in the treated and control groups culture medium samples (Fig. 6d). Additionally, the exposition to both doses seems to impact nearly in the same way the metabolites levels in the cells extracts and those found in the culture medium, except for culture medium data of FN1 at the same incubation time that revealed that the 50 µM molar concentration impacted much more incisively the composition. Considering that all experimental parameters were kept the same for the cultures of both cell lineages, such differences were tentatively attributed to the genetic origin of cells.

Among all the VIP scores obtained in the multivariate data analysis, each one was ascribed to a specific metabolite. Only those with statistical significance ($p < 0.05$) were retained in the metabolic evaluations. We used parametric and nonparametric methods chosen according to the data normality distribution [27,28]. Data were numerically tabulated, and heat maps were used to demonstrate the percentage shifts of increase (positive %) and decrease (negative %) in the levels of the significant VIP scores, i.e., the discriminant metabolites. For this purpose, the metabolites levels of the control samples were adopted as reference (no shift). The obtained results are summarized in Tables 2 and 3. Accordingly, those data provide a comprehensive impact of AgNP cytotoxicity on the endometabolome and exometabolome of the treated as compared with the respective control cells.

Moreover, the set of significantly impacted identified metabolites provide a clue on the possible metabolic pathways. It characterized the dynamic of biochemical transformations in the cells, demonstrating their metabolic response to the treatments with AgNP. For instance, it was possible to infer the cell lipid membrane composition and oxidative metabolism occurring in the mitochondria [21,22], as discussed below.

Discussion

It is known that cells from different lineages, each one playing a specific complementary function, are recruited by the organism to the wound environment during the healing of injured tissues to fulfill the process. Despite being highly integrated, the chain of biochemical events triggered by these cells follows a specific order, starting with an inflammatory step, then a proliferative step, and finishing with a remodelative step [7,29]. Therefore, if such events could be controlled by up- and down-regulation of vital metabolic pathways involved in the healing process simply by adjusting the concentration and treatment time with therapeutics, in principle, we could accelerate and optimize the process and prevent the undesirable formation of keloids. The present work was proposed considering silver nanoparticles, a nanomaterial that has proven to be beneficial in accelerating the healing process for such a purpose, based on standard cytotoxic assays and evaluation of the biochemical transformations by nuclear magnetic resonance spectroscopy. The temporal dynamic of the metabolomes of two cell lineages was characterized by an approach known as "metabolic profiling" [22], where the significant results for the identified metabolites are summarized in the tables 2 and 3, respectively, for FN1 and HUV-EC-C cells as discussed hereon. The access to such metabolomic information as a function of the AgNP concentration and treatment time allowed us to evaluate their impact on the cell metabolism and the dose- and time-dependent cytotoxicity mechanisms. From the data, the sensitized metabolic pathways were successfully identified.

Although we did not achieve direct evidence of pyruvate in the magnetic resonance spectra, we can access the glycolytic cell's activity by probing the levels of glucose, lactate, succinate, and, additionally, AcOH, the last one resultant from pyruvate oxidation. Both the endo- and the exometabome provide valuable information showing that AgNP can play a dose- and time-dependent role in this metabolic pathway; in other words, in how treated cells produce biochemical energy (ATP molecules). Pyruvate molecule is the end product of glycolysis (see Fig. 9) that can diverge towards aerobic pathways through its decarboxylation leading to the coenzyme acetyl-CoA, a primary substrate for the TCA, to produce two ATP molecules and electron carrier coenzymes that can follow the mitochondrial oxidative phosphorylation metabolism yielding approximately 15 times more ATP molecules to the cells [30]. Succinate molecules, detected in exometabolome (culture medium samples), provide direct evidence of activation of TCA upon being produced in the cycle from the release of succinyl-CoA coenzyme molecules, producing just one ATP molecule in this process. Our data reveal that FN1 cells present an abundance of succinate in the media sample (about 11%) of the treated cells, suggesting a slight down-regulation at this point of the cycle. The cells have other energetically less efficient mechanisms to drive the pyruvate molecule, and for instance, it can follow anaerobic pathways being converted into lactate through lactic acid fermentation. Furthermore, pyruvate can be simply oxidized by cells transformed into acetate (AcOH). Both lactate and AcOH were detected in cell extracts and culture media of treated FN1 and HUV-EC-C cells in both incubation times, and their correspondent levels were consistent with a tendency to oxidize the pyruvate rather than activate the ATP production using the lactic acid fermentation pathway, thus suggesting that AgNP is inducing cells to an energy waste condition. The direct evaluation of glucose consumption from the exometabolome data indicated that the treatment is

up-regulating the glycolytic metabolism of cells to produce pyruvate to the detriment of energy, as discussed above.

Furthermore, FN1 cells incubated for 24 hours showed a progressive dose-dependent tendency to waste glucose molecules left over in the cell environment. These results and considerations are consistent with an impairment of energetic metabolism of the cells that exhibited higher demand for more glucose, which are oxidized to pyruvate and AcOH, consequently producing fewer ATP molecules. Starving cells usually seek alternative metabolic routes to supply their energy needs when the conventional ones are saturated for any reason, in this case, due to the cytotoxicity of AgNP. For instance, acetone is a molecule resulting from ketogenesis metabolism (see Fig. 9). Two molecules of acetyl-CoA coenzyme diverge from the TCA to produce acetoacetyl-CoA, which is transformed into -hydroxybutyrate and acetoacetate, finally leading to acetone. These molecules are considered ketone bodies [31]. The endometabolome data reveal a surplus of acetone excreted to the medium by treated FN1 and HUV-EC-C cells responding to such a stressful condition by up-regulating this specific metabolic pathway, especially during the first 24 hours of incubation (about 130% higher than control). Finally, cells can use intracellular levels of creatine (and phosphocreatine), detected in the endometabolome data, for temporal and spatial energy buffering by activating the PCR/Cr-shuttle metabolism [32]. The phosphocreatine could not be directly found, but the creatine levels suggest its breakdown into creatine and inorganic phosphates for ATP synthesis. We observed a general tendency of treated FN1 and HUV-EC-C cells, in both incubation times, to decrease creatine production, except in one specific case where FN1 cells were treated with 50 μM of AgNP for 24 hours. This observation enables us to suggest that the cytotoxicity induced by AgNP forces cells to a situation of high metabolic energetic demand when the rate of ATP use overwhelms its production by other metabolic pathways [33] as we discussed before for the TCA, oxidative phosphorylation, and ketogenesis metabolisms.

Some aminoacids detected in endometabolome data provide essential indicators of a protein degradation process that may be occurring in treated cells. For instance, the levels of leucine, isoleucine, glycine, alanine, and glutamate generally tend to decrease in the endometabolome data upon treatment of FN1 and HUV-EC-C cells for 24 and 48 hours. Nevertheless, for the specific case of leucine, an increase in its levels was observed after incubation for 24 hours for both cell lineages. The exometabolome data of both cell lineages showed that the aminoacids leucine, isoleucine, phenylalanine, and methionine had their levels systematically increased as a function of AgNP dose for both incubation times, suggesting a lowering in their respective consumption rates by cells. The exception was detected for the alanine that had its level decreased in the lineages treated for 24 hours. Independently of the origin of such aminoacids, whether from protein degradation or the culture media, all of them can be readily used by cells in the convergent biosynthesis of a few high energy substrates by a breakdown of their respective carbon chains in oxidative processes typical of aminoacid metabolism [34]. For instance, pyruvate can be produced from alanine and glycine, acetyl-CoA from leucine, isoleucine, phenylalanine, succinyl-CoA from methionine, and fumarate from phenylalanine. Cells can use these substrates to replenish TCA cycle intermediates and thus rebalance the entire cycle when needed. Given the reduced levels of alanine and

glycine in the endometabolome, we could suggest that more pyruvate can be synthesized by treated cells to fulfill their needs, as discussed before, in the TCA or the oxidative pathway. Leucine and isoleucine follow a similar tendency of decreased levels. It is plausible that these aminoacids are being used by treated cells to produce more acetyl-CoA than the control cells. In contrast, the exometabolome data indicate an opposite situation where fewer aminoacids from the culture medium are being used by treated cells to produce intermediates for the TCA. This apparent complex picture that emerges from both metabolomes of treated cells seems to point out that, in general, the AgNP inherent cytotoxicity is causing a blockage of TCA even though pyruvate and acetyl-CoA production remains almost unchanged.

The level of pyroglutamate shown in exometabolome data presents a consistent decreasing tendency in treated FN1 and HUV-EC-C cells as the dose of AgNP increases, independently of the incubation time. One molecule of nicotinamide adenine dinucleotide phosphate (NADPH) is oxidized to NADP+ (Forman et al., 2009). That molecule is an intermediate glutathione biosynthesis excreted by cells to the media, which plays an essential role in reducing inactive oxidized proteins by removing disulfide bridges, and in regenerating SH groups oxidized, for instance, ROS, thus reestablishing their original functions in the cells. N-Acetylcysteine, the N-acetyl derivative of L-cysteine, an organic compound belonging to the N-acyl-alpha aminoacids, is an important precursor of pyroglutamate as well as glutathione [35]. Clearly, the level of this metabolite also showed a tendency to decrease for both treated cells and incubation times. If less pyroglutamate is being excreted by cells to the culture medium and less N-Acetylcysteine is found in the cellular environment compared to the control, thus treated cells are probably driving their metabolism to elevate the production of antioxidant agents such glutathione (see Fig. 9). Considering that compelling evidence for this mechanism was identified and quantified, it is possible to infer that cells are suffering different levels of oxidative stress induced by AgNP as a function of its dose, where the endothelial cells demonstrated to be more sensitive than the fibroblast cells.

Formate, the simplest carboxylic acid that participates in the metabolism of one-carbon compounds, generally undergoing transmethylation reactions, can be responsible for signaling the disruption of the mitochondrial electron transport chain in oxidative phosphorylation metabolism, thus impacting the cell capacity to produce energy by inhibiting the cytochrome-c oxidase activity [36]. As this excreted metabolite had its levels decreased in the exometabolome of treated FN1 and HUV-EC-C cells at both incubation times, we would expect that the formate is probably down-regulating the cytochrome coenzyme when compared to the control and thus signalizing an impairment of mitochondria functionalities to produce energy.

Phospholipid metabolism can be accessed by changes in O-Phosphocholine and Sn-Glycerol-3-PC levels in the endometabolome of treated cells (see Fig. 9). These metabolites are essential components of cellular membranes synthesized from choline in the culture medium and catalyzed by CTP synthetase [37]. Although we had detected free choline in the exometabolome of FN1 cells only after 48 hours of incubation, both molecules were found in the endometabolome of the two cell lineages and demonstrate a general tendency to reduce their levels as a function of the dose of AgNP used in the treatment. This behavior suggests that the cytotoxicity of the nanoparticles, which induced cell death, is down-regulating

the phospholipid metabolism and, consequently, lowering the rates of cell proliferation, as observed in the results obtained from cytotoxicity assays, which are summarized in Fig. 1 and Fig. 2.

Other metabolic pathways of cells sensitized by AgNP could also be detected based on some critical metabolites identified in the endo- and exometabolome. For instance, propylene glycol levels progressively decreased in the exometabolome of both treated cells in both incubation times. This metabolite can be used in the cellular propanoate metabolism to produce propanoyl-CoA by condensing the thiol group of CoA with the carboxyl group of propionic acid (propanal) [38]. Depending on the cell's need, propanol-CoA can eventually lead to the formation of succinyl-CoA, an important intermediate in TCA. This observation supports our premise that AgNP impacts this specific part of the energetic metabolism, the TCA, by down-regulating some of its biochemical intermediates. N-Acetylglutamate and N-Acetylaspartate are two metabolites excreted by treated HUV-EC-C cells. They present a systematic increase in their levels compared to the control, as shown in the correspondent exometabolome. Both these metabolites play a role in the aminoacid biosynthesis metabolism [36] and provide evidence that the type/nature of cells influences the resistance to the cytotoxic effects of AgNP, as observed previously in the cytotoxic assays, reinforcing the validity of the metabolomic results. Cadaverine, another metabolite excreted only by HUV-EC-C cell lineage, presents lower levels when compared to control, as shown in the correspondent exometabolome. This metabolite is the first subproduct of lysine degradation formed by bacterial decarboxylation that occurs in the metabolism of aminoacids and usually is associated with protein hydrolysis during the putrefaction of animal tissues [36]. Our data suggest that the lysine metabolism of HUV-EC-C cells is down-regulated by the dose and time of AgNP treatments almost in the same way as the control.

To conclude the analysis of the metabolites that changed with the treatment with silver nanoparticles, the uridine diphosphate-N-acetylglucosamine (UDP-GlcNAc), excreted by both cell lineages, as informed in the endometabolome data, is progressively decreased as the dose increase, except for 50 µM of AgNP and 24 hours incubation with FN1 cells. This metabolite plays a vital role in modifying nucleocytoplasmic proteins, acting as a donor substrate for serine and threonine residues linking N-acetylglucosamine (O-GlcNAc) to the naked proteins [36,39]. Our data show that AgNP treatment can induce changes in this class of protein, in general, inhibiting such modifications.

Conclusions

Dose- and time-dependent metabolic changes induced by AgNP on FN1 and HUV-EC-C cells were successfully identified in the cellular extracts samples (endometabolome) and the culture media samples (exometabolome). In general, treated cells from both lineages are up-regulating the glycolysis metabolism by consuming more glucose molecules. However, these treated cells are wasting the produced energetic pyruvate molecules by oxidation, as confirmed by the increasing AcOH levels. The TCA is down-regulated once succinate is left over by cells into culture media. At the same time, the ketogenic pathway is up-regulated since an excess of Acetone was detected in these samples. Additionally, the excess of unphosphorylated creatine molecules detected suggests cell attempts at temporal and spatial energy

buffering in the cellular environment. Aminoacids detected in the endometabolome of treated cells provide evidence that the protein degradation mechanism may be activated. In contrast, those found in the culture medium suggest down-regulation of aminoacid metabolism to produce intermediates to the TCA, although Pyruvate and Acetyl-CoA. However, the biosynthesis of this coenzyme from leucine, isoleucine, and phenylalanine remained almost unchanged.

Pyroglutamate and N-Acetylcysteine are intermediates of glutathione biosynthesis, an essential antioxidant agent; they are consistently changing as revealed, respectively, by the exometabolome and endometabolome data of both cell lineages. This behavior suggests that cells are responding to the oxidative stress caused by AgNP by increasing glutathione synthesis. The decreased formate levels in the exometabolome seem to corroborate the assumption that oxidative stress in treated cells impacts mitochondrial function.

The phospholipid metabolism is down-regulated in the treated cells incubated for 24 and 48 hours as suggested by the decrease of O-Phosphocholine and Sn-Glycerol-3-PC levels in the endometabolome data, signaling a reduction in the cell proliferation rate concurrently to the elevation in the cellular death rate. These results agree with the cytotoxicity data.

To the best of our knowledge, the analysis also revealed for the first time that UDP-GlcNAc, excreted by both lineages of cells, are changing in different ways in the treated cells when compared to the controls. As this metabolite plays a vital role in modifying nucleocytoplasmic proteins, the data suggest that AgNP treatment can directly impact this protein class, reducing such modifications.

The presented metabolic pathways respond to AgNP dose and treatment time in different ways compared to the controls, being up- or down-regulated as a function of the set of parameters used in the incubation, as demonstrated. Therefore, by adjusting these parameters, we could achieve, in principle, the control of some critical events that occur in the wound healing by controlling the cell behavior, for instance, the rate of cell proliferation, the mitochondrial activity, the production of antioxidant agents, the mechanism of cellular energy buffering, among others. In short, AgNP induced significant oxidative stress and cytotoxicity to endothelial and fibroblast cells, influencing their endo- and exometabolome, thus indicating that care should be taken during their use in choosing a suitable concentration to produce better healing without compromising healthy cells and tissues.

Materials And Methods

Silver nanoparticles. Stable dispersions of spherical-shaped AgNPs with 40-nm average diameter were synthesized using an adapted Turkevich method [40]. In this protocol, silver salt is refluxed with citric acid that acts by reducing and stabilizing the nanoparticles in the aqueous solution. The obtained solution presented a concentration of elemental silver, determined from ICP-OES, of 27.3 mg/L (250.3 μM). Briefly, 4.25 mg of silver nitrate (anhydrous ≥ 99.999% trace metals base, Sigma-Aldrich®, St. Louis, USA) was solubilized in 100 mL of ultrapure water (18 MΩcm) and heated. Then, 1 mL of a 0.5 molL^{-1} citric acid

solution (anhydrous, ≥ 99.5%, Sigma-Aldrich®) was added to the boiling silver solution and kept under stirring for 5 min. Then, the reaction mixture was cooled down to room temperature, filtered through a 0.2 μm sterile cellulose membrane syringe filter (Corning®, New York, USA), and diluted with ultrapure water to prepare the stock dispersion of nanoparticles used in work. The AgNP in the stock dispersion was dissolved with concentrated nitric acid and analyzed by ICP-OES to determine the actual concentration of elemental silver in the sample using a calibration curve generated using a standard analytical solution of silver (1000 ppm) in nitric acid. Samples for biological assay were prepared by dilution of the concentrated stock dispersion of AgNPs (250.3 μM of Ag) to 25, 50, 75, 100, and 185 μM of silver atoms with DMEM (Dulbecco's Modified Eagle Medium-high glucose, Gibco®, Waltham, USA) culture media supplemented with 10% (v/v) of fetal bovine serum (FBS, Gibco®), named from now on control medium (free of nanoparticles). The absolute number of nanoparticles was estimated from the molar concentrations, considering spherical nanoparticles with 40-nm average diameter possessing Hexagonal Close Packed Crystal Structure (HCP) and density of 7.9 g/cm^3, such that 25 μM corresponds to 1.0 × 10^{13} nanoparticles/L.

Cell culture. Human endothelial cells were acquired from American Type Culture Collection (ATCC®, Manassas, USA) with the following ATCC number and designations: CRL-1730™ and HUV-EC-C. Human normal fibroblast cells, designated as FN1, were provided by the Butantan Institute, Brazil. The cells were cultivated the same way for the experiments with those lineages and consisted of the following steps. First, a standardized stock of frozen cells containing approximately 2 × 10^6 cells, previously prepared enough to attend all experiments, was thawed at room temperature by dripping 1 mL of control medium preheated at 37 °C. In the sequence, the solution was used to inoculate one cell culture flask with a surface area of 25 cm^2 (T25 bottle) and left to expand for 48 hours in a commercial CO$_2$ incubator (Series II Water Jacket, Thermo Scientific, Waltham, USA). Then, the exhausted culture media was removed, the adhered cells washed with 5 mL of phosphate buffer saline solution (PBS, Sigma-Aldrich®) a couple of times, and detached from the bottle by adding 1 mL of 1×trypsin-EDTA solution (Sigma-Aldrich®). The cells in suspension were counted, separated into two equal aliquots, transferred to two T75-bottles (surface area of 75 cm^2), and left to expand for additional 48 hours to get 20 mL of cells at approximately 2 × 10^6 cells/mL, that was diluted with control culture media and used in the assays. A similar procedure was adopted for all lineages of cells.

Cellular growth kinetic (CGK). The cellular growth kinetics was evaluated by monitoring the cell proliferation rates accounted for in a OptikLabor (Görlizt, Germany) Neubauer hemocytometer. The characteristic curve was plotted as a function of time. Seventy-two 220 μL aliquots of cells suspended in control media at a concentration of 1 × 10^5 cells/mL were transferred to a 96-well plate, one *per* lineage, and incubated for 12 hours at 37 °C to promote cellular adherence (stabilization phase). Control culture media were spiked with suitable volumes of AgNPs stock dispersion to get solutions with final silver concentrations of 0 (control), 25, 50, 75, 100, and 185 μM that were used to replace the exhausted culture media to treat the cells at incubation times of 24, 48, 72, and 96 hours. This assay was carried out in a triplicate scheme of samples: six concentrations × four times × three copies of samples (see Table 1).

Subsequently, the cells were harvested by conventional trypsinization, and the viable cells were manually counted using the *Neubauer Counting Chamber* (NCC).

Cytotoxicity. The cytotoxic effects of AgNPs at those same six concentrations were evaluated by estimating the cell proliferation rates in 500 μL at a concentration of 2×10^5 cells/mL and incubation times of 24 and 48 hours in quadruplicate in two plates of 24 wells *per* lineage (see Table 1), using the hemocytometer. As in the previous assay, cells were left to stabilize in the incubator under the same experimental conditions before starting the treatment.

Cellular metabolic activity (MTT assay). The cellular metabolic potential of treated cells was evaluated by MTT assay using a Biotek (PowerWave XS2, Vermont, USA) spectrophotometer. Thirty aliquots of 220 μL and a concentration of 1×10^5 cells/mL were transferred to a 96-well plate and incubated for 12 h to stabilize the cells and subsequently treated with 0 (control), 25, 50, 75, 100, and 185 μM of AgNPs in control culture media for 24 (and 48 hours in another 96-well plate), in quintuplicate: six concentrations × two times × five copies of samples (see Table 1). Then, the cells were rinsed three times with PBS before adding 100 μL of 0.5 mg/mL of yellow tetrazolium MTT salt (Sigma-Aldrich®, 3-(4,5-dimethyl-2-thiazolyl)-2,5-diphenyl-2H-tetrazolium bromide) dissolved in control media. After 2 hours of incubation at 37 °C, the MTT solution was fully removed, the adhered cells were washed with water, and the remaining insoluble dark purple formazan crystals were dissolved with 100 μL of DMSO (Dimethyl sulfoxide, Merck KGaA, Darmstadt, Germany). Plates were placed in the spectrophotometer, and the absorbance at 570 nm was measured at 24 °C. Four consecutive runs were performed to add statistical significance to the results.

Proton nuclear magnetic resonance (^{1}H-NMR). Cellular metabolic status was evaluated by proton magnetic resonance spectroscopy of cellular extracts and metabolized culture media. In these experiments, 60 aliquots of 1500 μL containing 2.5×10^5 cells/mL and 3.0×10^5 cells/mL of FN1 and HUV-EC-C were seeded in ten plates of six wells, one set of plates *per* lineage. Plates were transferred to the incubator and left for 12 hours to stabilize the cells before starting the treatment with silver nanoparticles. After stabilization, the wells were depleted, washed with 2 mL of PBS, and 1.5 mL of control media containing 0 (control), 25, 50, 75, and 100 μM of AgNPs were transferred to the respective wells. Six replicates were prepared for each concentration, i.e., one six-well plate for each concentration where a set of five plates were incubated for 24 and, separately, another set of five plates were incubated for 48 hours to evaluate the effects of time and concentration of nanoparticles on cell metabolism (see Table 1).

Subsequently to the cultivation phase, cells and media follow distinct paths to produce the samples for magnetic resonance evaluation of this work. The content of each well with harvest culture media sample was transferred to 2 mL microcentrifuge tubes (Corning®), centrifuged for 6 min and 1300 r.p.m. at room temperature to deposit large particles and debris. Aliquots of 1.5 mL of supernatant were then collected, transferred to lyophilization vials, frozen at -80 °C, and lyophilized for 24 hours. Meanwhile, cells in the bottom of wells were washed with 2 ml of PBS, detached using 250 μL of trypsin, and transferred to

microcentrifuge tubes for the metabolic extraction process [22]. First, the contents of the tubes were centrifuged in the same conditions as before, the supernatant discarded, PBS added to wash the cells, and centrifuged again. This step was repeated twice or more to completely remove culture media and trypsin residues whose signals could unduly appear in the magnetic resonance spectra. After purifying the cells, 1 mL of a cold methanol-water mixture (1:1) was added for each well and submitted to 5 or 6 cycles of 30 s ultrasound treatment separated by 5 min to promote cell lysis and interruption of cellular metabolism. The resultant solutions were centrifuged at 2000 RPM (revolutions per minute) and 4 $^{\circ}$C for 90 min to separate debris from non-lysed cells. Supernatants were collected, aliquoted with about 850 µL, frozen, and then lyophilized for 24 hours. The lyophilized extracts, culture medium, and cells were diluted with 500 µL of deuterium oxide (D$_2$O, Sigma-Aldrich®) containing 4,4-dimethyl-4-silapentane-1-sulfonic acid (DSS, Sigma-Aldrich®) at 5.0 mM for culture media and 0.5 mM for cellular extracts, respectively, and finally transferred into 5 mm sample tubes, immediately prior to the magnetic resonance experiments.

The ^{1}H-NMR experiments were performed in a Varian spectrometer (Varian Inc., Palo Alto, CA, USA) with three channels and pulsed-field gradients, coupled to a 5 mm triple resonance probe (^{1}H, ^{13}C, ^{15}N) operating at a constant frequency of 399.7 MHz for protons nuclei. Spectra were acquired using a combination of the NOESY-1D pulse sequence and selective saturation of residual water. Some experimental conditions were kept constant during the FID acquisitions from samples of cellular extracts and culture media: temperatures of 25 $^{\circ}$C, spinning rates of 20 Hz, relaxation delays of 1.0 s, 7.5 µs wide excitation pulses, mixture time of 150 ms, and approximately 2 s wide selective water saturation pulse applied at 4.7 ppm respective to DSS. For cell samples, a spectral window of 10 ppm, with 16384 complex points and 1228 transients *per* signal, is equivalent to approximately two and a half hours of acquisition. A spectral window of 12 ppm, with 38460 complex points and 164 transients *per* signal, equivalent to approximately sixteen minutes of the acquisition, was used for culture media samples. Line broadening of 0.3 Hz was applied on Fourier transformation of FID, followed by phase adjustment and baseline correction through spline curves to generate spectra in absorptive mode. Magnetic field homogenization through shimming procedures was performed before each acquisition to ensure a suitable spectral resolution to achieve line width at half height (LWHH) values of the DSS in the 0.5 to 1.5 Hz range. Spectral signal-to-noise ratios (SNRs) were calculated and used to determine the level of uncertainty of the measurements resulting in 383 ± 230 and 6375 ± 2508, respectively, for cellular and culture medium samples. The spectra were normalized two times to fulfill the statistical analysis requirements as follows: first, the chemical shifts x-axis was adjusted, setting the DSS signal to 0 ppm and rescaling the y-axis by adjusting the DSS area to the correspondent concentration of this reference molecule in the samples, i.e., 0.5 mM for cellular extracts and 5.0 mM for culture medium. The second spectral normalization was carried out by determining the total peak area in the 0.7 to 8.6 ppm range without considering the interval of residual water signal found at 4.2 to 5.5 ppm, dividing their intensities by the corresponding areas. These actions prevent a) issues regarding alterations in the sample's pH that could shift the high-resolution lines and slight alterations in the gain of the resonance spectrometer that could distort the signal intensities (first normalization); and b) changes in the lyophilized mass of cells or

media from eventual biological variability that could influence the composition of metabolite areas in the spectra (second normalization) [22,24,41].

Table 1

The strategy used for preparation of the samples *per* cellular lineage, FN1 and HUV-EC-C, indicating the doses, incubation times, and the number of replicates to cultivate the cells in the presence of AgNP.

experiment	doses (µM)	incubation times (hours)	replicates per dose	total of cultivated wells
CGK	0/25/50/75/100/185	24/48/72/96	3	72
cytotoxicity	0/25/50/75/100/185	24/48	4	48
MTT	0/25/50/75/100/185	24/48	5	60
^{1}H-NMR	0/25/50/75/100	24/48	6	60

Statistical data analysis. For the cell viability studies, statistical analyses were performed using the Student's T-test, setting a confidence level of 95% ($p < 0.05$). The linear and non-linear estimation methods were used to calculate the proliferating cellular rates, τ, from the number of viable cell counts in the Neubauer chamber. The half-maximal effective concentrations, EC50 parameters, were estimated from MTT data and accounted for those concentrations of AgNPs that promote a reduction in the number of cells with mitochondrial activity to half.

For the metabolomic study, Partial Least Squares-Discriminant Analysis (PLS-DA) was used as a supervised multivariate method suitable to detect small changes in the systems under analysis [24–26]. Input variables, represented by the metabolites areas corresponding proportionally to their respective concentrations, or levels, were mean-centered and divided by their correspondent standard deviation to prevent huge differences among the areas' magnitudes that could result in imprecise results. The generated models were composed of four components: computing predictions and displaying results; seven steps of cross-validation groups; 95% confidence level of parameters; and a 0.05 significance level of Hotelling's T2 ellipses [42]. Scores plot, showing the tendencies of similar samples represented as clusters of points in 2D coordinate space (Comp. 1 *vs.* Comp. 2; Comp. 1 *vs.* Comp. 3; Comp. 2 *vs.* Comp. 3), and Variables of Importance in Projection (VIP), showing the classifying metabolites, or areas, in descending order, were carefully analyzed to proceed to the univariate statistical analyses necessary to establish the statistical relevance of the multivariate method. Parametric univariate ANOVA-coupled Fisher's pairing and nonparametric Kruskal-Wallis tests, suitable for comparisons of more than three different groups, were chosen by data normality checking through the Anderson-Darling test assuming null hypothesis as a normal distribution (Massad et al. 2004; Heckler 2005). All statistical analyses and plots were performed in *Minitab* (Minitab Inc., institutional license, State College, PA), SIMCA-P (Umetrics™, trial license, Malmö, Sweden), and Microcal Origin (© OriginLab Corporation., Northampton, MA, USA).

Declarations

Data availability. The data set used and/or analyzed in this work are available from the corresponding author on reasonable request.

Competing Interests Statement. The author(s) declare no competing interests.

References

1. Lee, W., Kim, K.-J. & Lee, D. G. A novel mechanism for the antibacterial effect of silver nanoparticles on Escherichia coli. *Biometals* **27**, 1191–1201 (2014).

2. Manjumeena, R., Duraibabu, D., Sudha, J. & Kalaichelvan, P. T. Biogenic nanosilver incorporated reverse osmosis membrane for antibacterial and antifungal activities against selected pathogenic strains: an enhanced eco-friendly water disinfection approach. *J. Environ. Sci. Health A Tox. Hazard. Subst. Environ. Eng.* **49**, 1125–1133 (2014).

3. Lara, H. H., Ayala-Nuñez, N. V., Ixtepan-Turrent, L. & Rodriguez-Padilla, C. Mode of antiviral action of silver nanoparticles against HIV-1. *J. Nanobiotechnology* **8**, 1 (2010).

4. Eby, D. M., Luckarift, H. R. & Johnson, G. R. Hybrid antimicrobial enzyme and silver nanoparticle coatings for medical instruments. *ACS Appl. Mater. Interfaces* **1**, 1553–1560 (2009).

5. Tian, J. *et al.* Topical delivery of silver nanoparticles promotes wound healing. *ChemMedChem* **2**, 129–136 (2007).

6. You, C. *et al.* Silver nanoparticle loaded collagen/chitosan scaffolds promote wound healing via regulating fibroblast migration and macrophage activation. *Sci. Rep.* **7**, 10489 (2017).

7. de Lima, R., Seabra, A. B. & Durán, N. Silver nanoparticles: a brief review of cytotoxicity and genotoxicity of chemically and biogenically synthesized nanoparticles. *J. Appl. Toxicol.* **32**, 867–879 (2012).

8. Lansdown, A. B. G. Silver in health care: antimicrobial effects and safety in use. *Curr. Probl. Dermatol.* **33**, 17–34 (2006).

9. AshaRani, P. V., Low Kah Mun, G., Hande, M. P. & Valiyaveettil, S. Cytotoxicity and genotoxicity of silver nanoparticles in human cells. *ACS Nano* **3**, 279–290 (2009).

10. Hackenberg, S. *et al.* Silver nanoparticles: evaluation of DNA damage, toxicity and functional impairment in human mesenchymal stem cells. *Toxicol. Lett.* **201**, 27–33 (2011).

11. Gojova, A. *et al.* Induction of inflammation in vascular endothelial cells by metal oxide nanoparticles: effect of particle composition. *Environ. Health Perspect.* **115**, 403–409 (2007).

12. Kang, K. *et al.* Vascular tube formation and angiogenesis induced by polyvinylpyrrolidone-coated silver nanoparticles. *Toxicol. Lett.* **205**, 227–234 (2011).

13. Kalishwaralal, K. *et al.* Silver nanoparticles inhibit VEGF induced cell proliferation and migration in bovine retinal endothelial cells. *Colloids Surf. B Biointerfaces* **73**, 51–57 (2009).

14. Grosse, S., Evje, L. & Syversen, T. Silver nanoparticle-induced cytotoxicity in rat brain endothelial cell culture. *Toxicol In Vitro* **27**, 305–313 (2013).

15. Arora, S., Jain, J., Rajwade, J. M. & Paknikar, K. M. Cellular responses induced by silver nanoparticles: In vitro studies. *Toxicol. Lett.* **179**, 93–100 (2008).

16. Rigo, C. *et al.* Active silver nanoparticles for wound healing. *Int. J. Mol. Sci.* **14**, 4817–4840 (2013).

17. Foldbjerg, R. *et al.* PVP-coated silver nanoparticles and silver ions induce reactive oxygen species, apoptosis and necrosis in THP-1 monocytes. *Toxicol. Lett.* **190**, 156–162 (2009).

18. Carlson, C. *et al.* Unique cellular interaction of silver nanoparticles: size-dependent generation of reactive oxygen species. *J. Phys. Chem. B* **112**, 13608–13619 (2008).

19. Li, N., Xia, T. & Nel, A. E. The role of oxidative stress in ambient particulate matter-induced lung diseases and its implications in the toxicity of engineered nanoparticles. *Free Radic. Biol. Med.* **44**, 1689–1699 (2008).

20. Park, M. V. D. Z. *et al.* The effect of particle size on the cytotoxicity, inflammation, developmental toxicity and genotoxicity of silver nanoparticles. *Biomaterials* **32**, 9810–9817 (2011).

21. Carrola, J. *et al.* Metabolomics of silver nanoparticles toxicity in HaCaT cells: structure-activity relationships and role of ionic silver and oxidative stress. *Nanotoxicology* **10**, 1105–1117 (2016).

22. Bacchi, P. S. *et al.* Metabolism under hypoxia in Tm1 murine melanoma cells is affected by the presence of galectin-3, a metabolomics approach. *Springerplus* **3**, 470 (2014).

23. Burova, I. *et al.* A parameterised mathematical model to elucidate osteoblast cell growth in a phosphate-glass microcarrier culture. *J. Tissue Eng.* **10**, 2041731419830264 (2019).

24. Bloise, A. C. *et al.* Discriminating aspects of global metabolism of neonatal cardiomyocytes from wild type and KO-CSRP3 rats using proton magnetic resonance spectroscopy of culture media samples. *In Vitro Cell Dev Biol Anim* **56**, 604–613 (2020).

25. Madsen, R., Lundstedt, T. & Trygg, J. Chemometrics in metabolomics–a review in human disease diagnosis. *Anal. Chim. Acta* **659**, 23–33 (2010).

26. Worley, B. & Powers, R. Multivariate analysis in metabolomics. *Curr. Metabolomics* **1**, 92–107 (2013).

27. Heckler, C. E. Applied Multivariate Statistical Analysis. *Technometrics* **47**, 517–517 (2005).

28. Massad, E., de Menezes, R. X., Silveira, P. S. P. & Ortega, N. R. S. *Métodos Quantitativos em Medicina*. (Manole, 2004).

29. Kwan, K. H. L. *et al.* Modulation of collagen alignment by silver nanoparticles results in better mechanical properties in wound healing. *Nanomedicine* **7**, 497–504 (2011).

30. Watt, I. N., Montgomery, M. G., Runswick, M. J., Leslie, A. G. W. & Walker, J. E. Bioenergetic cost of making an adenosine triphosphate molecule in animal mitochondria. *Proc Natl Acad Sci USA* **107**, 16823–16827 (2010).

31. Misra, S. & Oliver, N. S. Utility of ketone measurement in the prevention, diagnosis and management of diabetic ketoacidosis. *Diabet. Med.* **32**, 14–23 (2015).

32. Schlattner, U., Tokarska-Schlattner, M. & Wallimann, T. Mitochondrial creatine kinase in human health and disease. *Biochim. Biophys. Acta* **1762**, 164–180 (2006).

33. Wallimann, T., Wyss, M., Brdiczka, D., Nicolay, K. & Eppenberger, H. M. Intracellular compartmentation, structure and function of creatine kinase isoenzymes in tissues with high and fluctuating energy demands: the "phosphocreatine circuit" for cellular energy homeostasis. *Biochem. J.* **281 (Pt 1)**, 21–40 (1992).

34. Kanehisa, M., Furumichi, M., Sato, Y., Ishiguro-Watanabe, M. & Tanabe, M. KEGG: integrating viruses and cellular organisms. *Nucleic Acids Res.* **49**, D545–D551 (2021).

35. Chong, J. *et al.* MetaboAnalyst 4.0: towards more transparent and integrative metabolomics analysis. *Nucleic Acids Res.* **46**, W486–W494 (2018).

36. Wishart, D. S. *et al.* HMDB 4.0: the human metabolome database for 2018. *Nucleic Acids Res.* **46**, D608–D617 (2018).

37. Chang, Y.-F. & Carman, G. M. CTP synthetase and its role in phospholipid synthesis in the yeast Saccharomyces cerevisiae. *Prog. Lipid Res.* **47**, 333–339 (2008).

38. Wongkittichote, P., Ah Mew, N. & Chapman, K. A. Propionyl-CoA carboxylase - A review. *Mol. Genet. Metab.* **122**, 145–152 (2017).

39. Hart, G. W., Housley, M. P. & Slawson, C. Cycling of O-linked beta-N-acetylglucosamine on nucleocytoplasmic proteins. *Nature* **446**, 1017–1022 (2007).

40. Turkevich, J., Stevenson, P. C. & Hillier, J. A study of the nucleation and growth processes in the synthesis of colloidal gold. *Discuss. Faraday Soc.* **11**, 55 (1951).

41. Martins-Bach, A. B., Bloise, A. C., Vainzof, M. & Rahnamaye Rabbani, S. Metabolic profile of dystrophic mdx mouse muscles analyzed with in vitro magnetic resonance spectroscopy (MRS). *Magn. Reson. Imaging* **30**, 1167–1176 (2012).

42. Wu, Z., Li, D., Meng, J. & Wang, H. Introduction to SIMCA-P and Its Application. in *Handbook of Partial Least Squares* (eds. Esposito Vinzi, V., Chin, W. W., Henseler, J. & Wang, H.) 757–774 (Springer Berlin Heidelberg, 2010). doi:10.1007/978-3-540-32827-8_33.
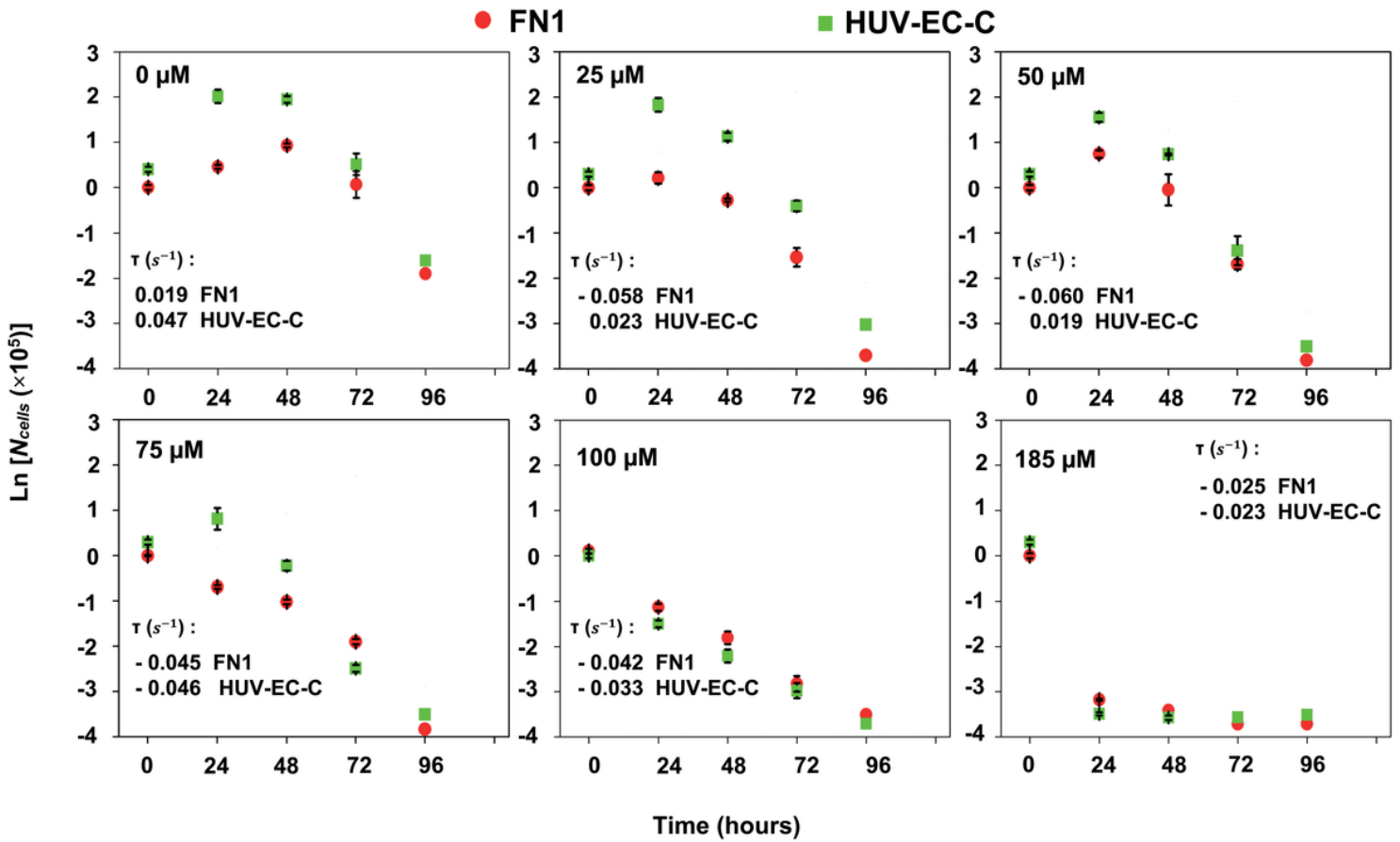
Figures

Figure 1

Natural logarithms of the number of viable FN1 (red circles) and HUV-EC-C (green squares) cells in control media were determined using a Neubauer chamber when incubated with increasing concentrations of AgNP (0 to 185 μM of silver) for up to 96 hours. Untreated cell lineages (in the absence of AgNP) were used as control.
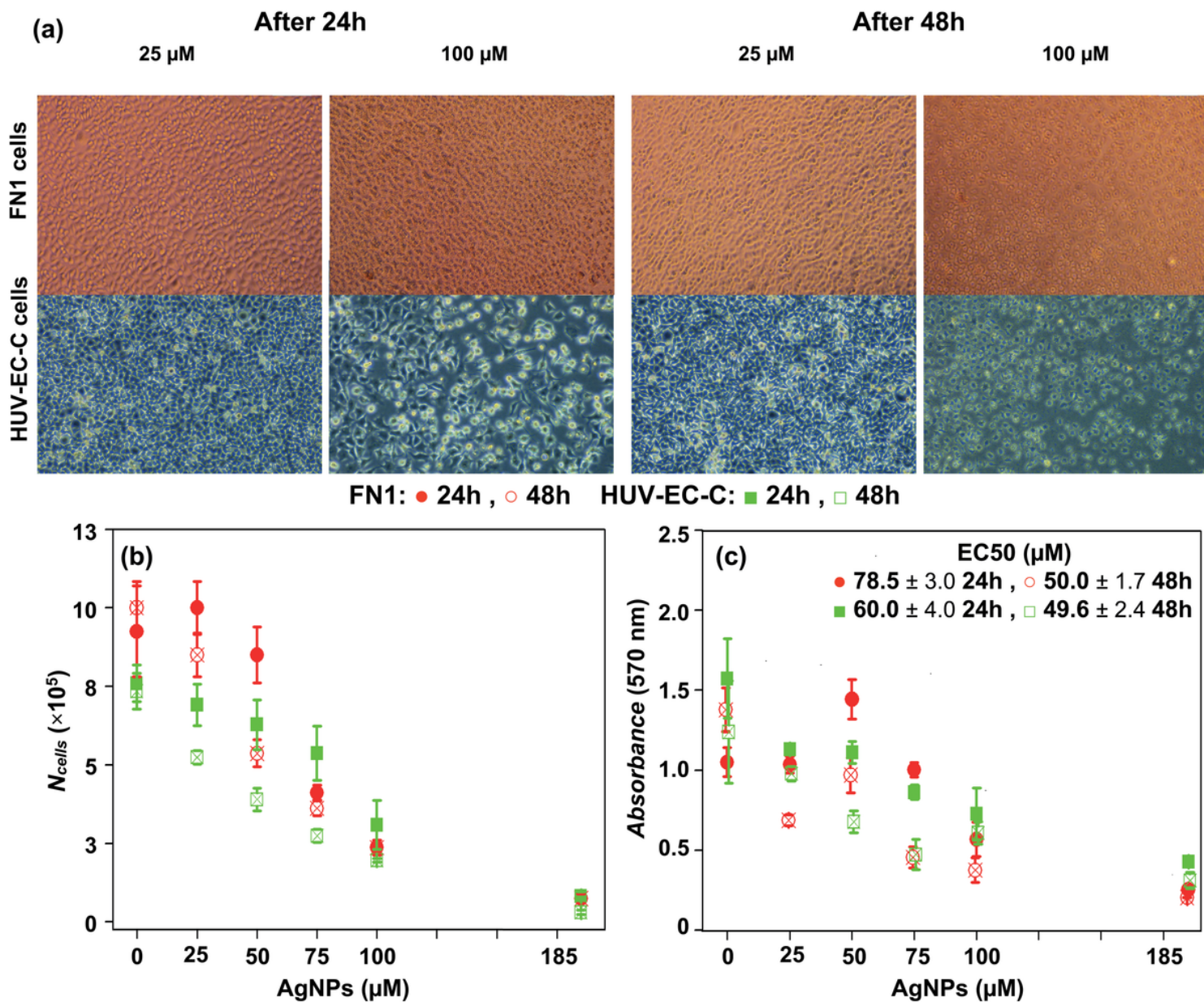
Figure 2

(a) Optical microscopies show the morphological aspects of FN1, upper row, and HUV-EC-C, bottom row, cells treated with 25 μM and 100 μM of AgNP for 24 hours (left) and 48 hours (right). The optical microscopies of cells incubated with 50 μM and 75 μM are shown in Figure 1a of Supplementary Information. (b) The number of viable cells counts in the Neubauer chamber and (c) the absorbance at 570 nm of MTT assays are plotted as a function of molar concentrations of silver in AgNP for FN1 (red circles) and HUV-EC-C (green squares) for 24 (filled symbols) and 48 hours of incubation time (open symbols); EC50 parameters were also included in this chart. The optical microscopies were obtained in an inverted Leica MC170HD microscope with ×10 magnification.
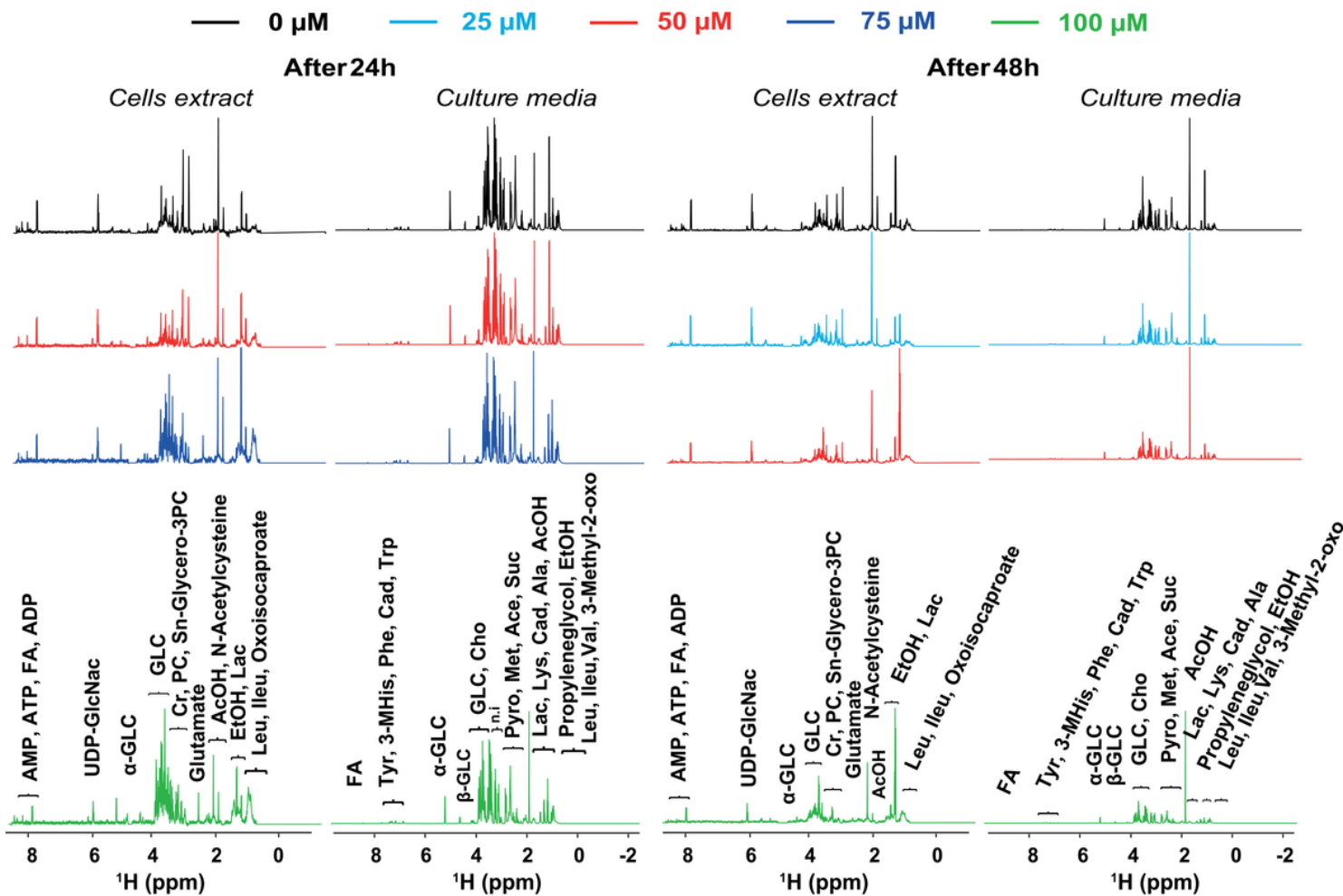
Figure 3

^{1}H-NMR high-resolution spectra obtained at 400 MHz and 25 °C for *cell extract* and *culture medium* samples of FN1 lineage treated with different molar concentrations of AgNP as follow: 0 µM or controls (black colored line), 25 µM (cyan), 50 µM (red), 75 µM (blue), and 100 µM (green). The left and right panels correspond to the results for 24 and 48 hours of cell incubation with silver nanoparticles at different concentrations. Seventeen metabolites were found in the cell extract samples: Creatine (Cr, δ 3.0; 3.9), Uridine diphosphate-N-acetylglucosamine (UDP-GlcNAc, δ 2.1; 3.8; 4.2; 4.4; 6.0; 8.3), O-Phosphocholine (PC, δ 3.2; 3.6; 4.2), N-Acetylcysteine (δ 2.1; 2.9; 4.4; 8.0), Sn-Glycerol-3-PC (GPC, δ 3.2; 3.6; 3.7; 3.9; 4.3), Glycine (Gly, δ 3.6), Lactate (Lac, δ 1.3; 4.1), Alanine (Ala, δ 1.4; 3.8), Isoleucine (Ileu, δ 0.9; 1.0; 1.2; 1.5; 1.9; 3.1), Leucine (Leu, δ 0.9; 1.7; 3.7), ADP (δ 4.2; 4.4; 4.6; 6.1; 8.3), AMP (δ 4.0; 4.4; 4.8; 6.1; 8.2), α-glucose (α-GLC, δ 5.2) and β-glucose (β-GLC, δ 4.6), 2-Oxoisocaproate (δ 0.9; 2.1; 2.6), Glutamate (δ 2.0; 2.1; 2.3; 2.4; 3.8), and Formate (FA, δ 8.4). In contrast, fourteen metabolites were found in the culture media samples: Formate (FA, δ 8.4), Lactate (Lac, δ 1.3; 4.1), Propilenglicol (EtOH, δ 1.2; 3.6), Acetate (AcOH, δ 1.9), α-glucose (α-GLC, δ 5.2), Leucine (Leu, δ 0.9; 1.7; 3.7), Isoleucine (Ileu, δ 0.9; 1.0; 1.2; 1.5; 1.9; 3.1), Methionine (Met, δ 2.1; 2.2; 2.6; 3.9), Phenylalanine (Phe, δ 3.1; 3.3; 4.0; 7.3; 7.4), Choline (Cho, δ 3.2; 3.5; 4.1), 3-Methyl-isovalerate (δ 0.9; 1.1; 1.4; 1.7; 2.9), Alanine (Ala, δ 1.4; 3.8), Pyroglutamate (Pyro, δ 2.0; 2.4; 2.5; 4.2; 7.7), and Succinate (Suc, δ 2.4). Chemical shift and intensity

standard: 4,4-dimethyl-4-silapentane-1-sulfonic acid (D_2O:DSS, 99.9%:1.0% w/w) not shown. The high-resolution spectra signals were assigned based on the metabolites databases provided in Chenomx NMR Suite (© Copyright 2009 - 2021 Chenomx Inc.) and the freely available electronic platform, The Human Metabolome Database (HMDB).
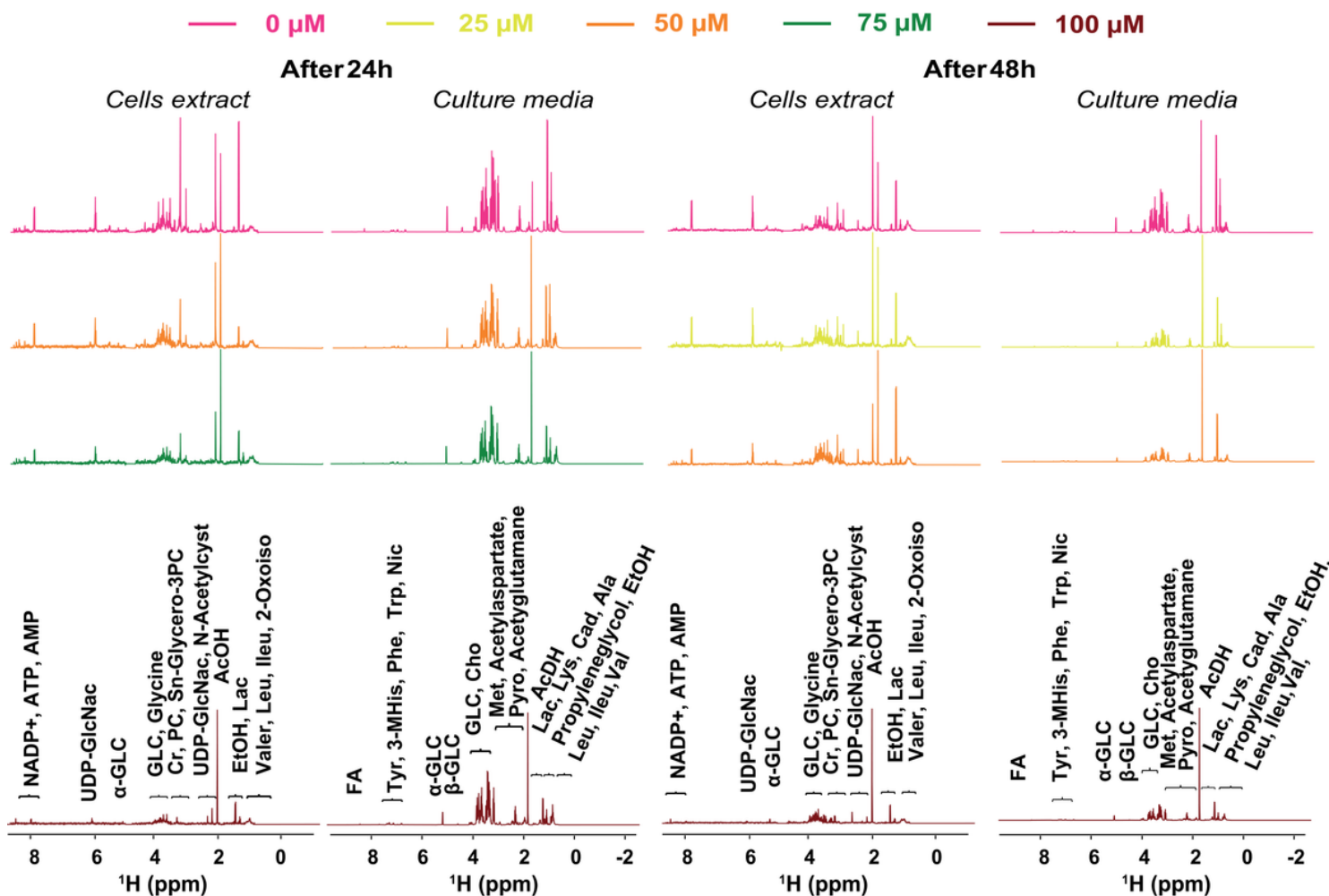

Figure 4

^{1}H-NMR high-resolution spectra obtained at 400 MHz and 25 °C for *cell extract* and *culture media* samples of HUV-EC-C lineage treated with different molar concentrations of AgNP as following: 0 μM, or controls (purple colored line), 25 μM (yellow), 50 μM (orange), 75 μM (dark green), and 100 μM (brown). The left and right panels correspond to the results for 24 and 48 hours of cell treatment with silver nanoparticles at different concentrations. Eighteen metabolites were found in the culture media samples: Creatine (δ 3.0; 3.9), Uridine diphosphate-N-acetylglucosamine (UDP-GlcNAc, δ 2.1; 3.8; 4.2; 4.4; 6.0; 8.3), O-Phosphocholine (PC, δ 3.2; 3.6; 4.2), N-Acetylcysteine (δ 2.1; 2.9; 4.4; 8.0), Sn-Glycerol-3-PC (GPC, δ 3.2; 3.6; 3.7; 3.9; 4.3), Glycine (Gly, δ 3.6), Lactate (Lac, δ 1.3; 4.1), Acetate (AcOH, δ 1.9), Valerate (Valer, δ 0.9; 1.3; 1.5; 2.2), Alanine (Ala, δ 1.4; 3.8), Isoleucine (Ileu, δ 0.9; 1.0; 1.2; 1.5; 1.9; 3.1), Leucine (Leu, δ 0.9; 1.7; 3.7), NADP^{+} (δ 4.2; 4.5; 6.0; 8.1; 8.2; 8.8), ADP (δ 4.2; 4.4; 4.6; 6.1; 8.3), AMP (δ 4.0; 4.4; 4.8; 6.1; 8.2), 2-Oxoisocaproate (δ 0.9; 2.1; 2.6), Glutamate (δ 2.0; 2.1; 2.3; 2.4; 3.8), and Formate (FA, δ 8.4). In

contrast, fifteen metabolites were found in the media samples at both exposition times: Formate (FA, δ 8.4), Lactate (Lac, δ 1.3; 4.1), Propilenglicol (EtOH, δ 1.2; 3.6), Acetone (δ, 2.2), Acetate (AcOH, δ 1.9), Cadaverine (Cad, δ 1.5; 1.7; 3.0), α-glucose (α-GLC, δ 5.2) and β-glucose (β-GLC, δ 4.6), Leucine (Leu, δ 0.9; 1.7; 3.7), Isoleucine (Ileu, δ 0.9; 1.0; 1.2; 1.5; 1.9; 3.1), Choline (Cho, δ 3.2; 3.5; 4.1), Alanine (Ala, δ 1.4; 3.8), Pyroglutamate (Pyro, δ 2.0; 2.4; 2.5; 4.2; 7.7), N-Acetylglutamate, and N-Acetylaspartate (δ 2.0; 2.5; 2.7; 4.4; 7.9). Chemical shift and intensity standard: 4,4-dimethyl-4-silapentane-1-sulfonic acid (D_2O:DSS, 99.9%:1.0% w/w) not shown. The high-resolution spectra signals were assigned based on the metabolites databases provided in Chenomx NMR Suite (© Copyright 2009 - 2021 Chenomx Inc.) and the freely available electronic platform, The Human Metabolome Database (HMDB).
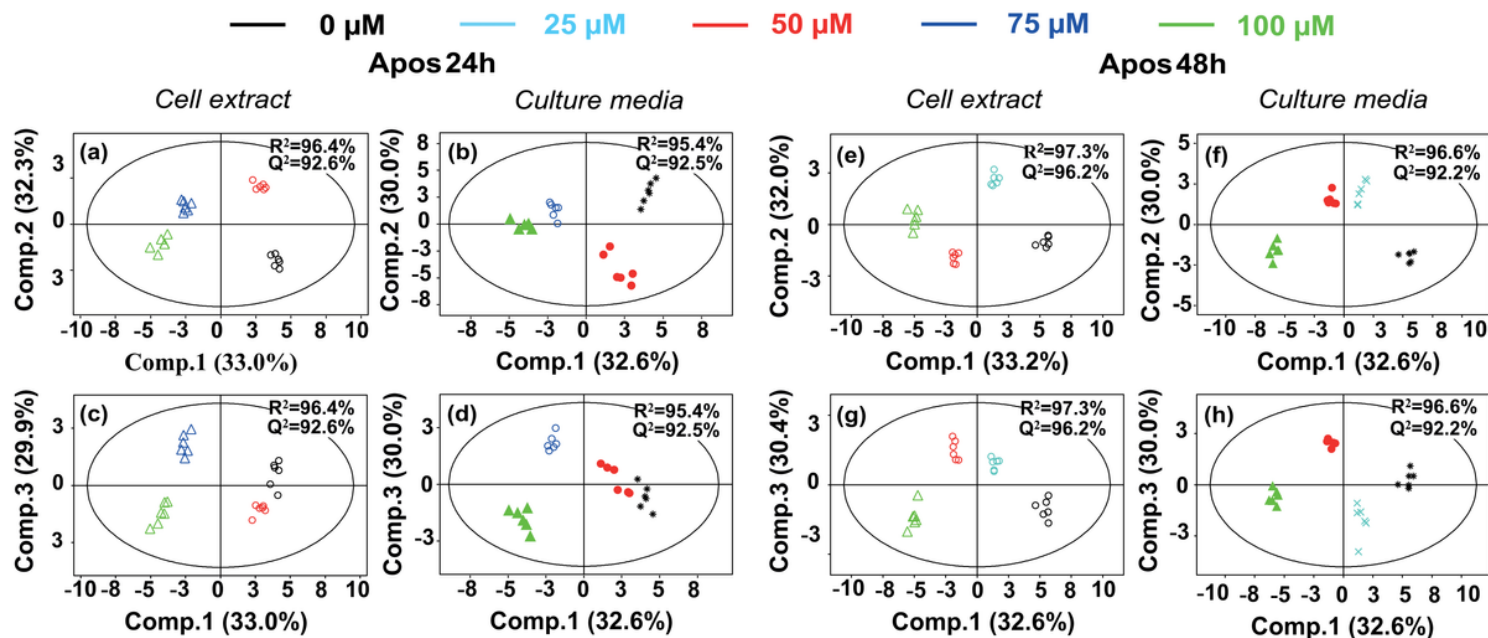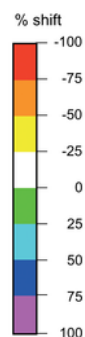

Figure 5

Summary of PLS-DA scores plots built using data obtained from the data analysis of *cell extract* and *culture media* samples from FN1 lineage incubated at different molar concentrations of AgNP as follows: 0 µM, or control (black colored labels), 25 µM (cyan), 50 µM (red), 75 µM (blue), and 100 µM (green). The four PLS-DA graphics on the left and right address, respectively, the results after 24 hours (a-d) and 48 hours (e-h) of treatment with silver nanoparticles, presenting columns corresponding to the cell extracts (a, c, e, g) and the culture media (b, d, f, h). In the brackets are shown the percentage of explained data covariance, the values obtained for R^2Y and Q^2 predictive parameters, and the tolerance ellipses based on Hotelling's T2.

Figure 6

Summary of PLS-DA scores plots based on the data analysis of *cell extract* and *culture media* samples from HUV-EC-C lineage incubated at different molar concentrations of AgNP: 0 µM or control (purple colored labels), 25 µM (yellow), 50 µM (orange), 75 µM (dark green), and 100 µM (brown). On the left and right of the figure are shown two panels, each one containing four PLS-DA graphics addressing, respectively, 24 hours (a-d) and 48 hours (e-h) of nanoparticles cell exposition, presenting one column dedicated to the cells (a, c, e, g) and another to the media (b, d, f, h). In the brackets are shown the percentage of explained data covariance, the values obtained for R^2Y and Q^2 predictive parameters, and the tolerance ellipses based on Hotelling's T2.

(a)

Incubation time (h)		24				48			
Molar concentration (μM)		0	50	75	100	0	25	50	100
Glycolysis	α-GLC	0.0	80.0	320.0	479.0	n.d.	n.d.	n.d.	n.d.
	Lactate	n.d.	n.d.	n.d.	n.d.	0.0	-24.0	-30.0	-42.0
	Alanine	n.d.	n.d.	n.d.	n.d.	0.0	-25.0	-26.0	-67.0
	Glycine	n.d.	n.d.	n.d.	n.d.	0.0	-24.0	-33.0	-51.0
Amino acids metabolism	Leucine	0.0	14.0	112.0	139.0	0.0	-15.0	-20.0	-27.0
	Isoleucine	n.d.	n.d.	n.d.	n.d.	0.0	-31.0	-37.0	-42.0
	Glutamate	0.0	3.0	-40.0	-58.0	n.d.	n.d.	n.d.	n.d.
Energy source	Creatine	0.0	26.0	-70.0	-86.0	0.0	-27.0	-40.0	-89.0
Phospholipid metabolism	O-Phosphocholine	0.0	79.0	-51.0	-84.0	0.0	-27.0	-19.0	-60.0
	Sn-Glycero-3-PC	0.0	10.0	-36.0	-82.0	0.0	-34.0	-46.0	-61.0
Antioxidant agent	N-Acetylcysteine	0.0	27.0	-22.0	-55.0	0.0	-21.0	-26.0	-47.0
	UDP-GlcNAc	0.0	10.0	-54.0	-76.0	0.0	-22.0	-35.0	-57.0
	AMP	n.d.	n.d.	n.d.	n.d.	0.0	-38.0	-47.0	-52.0
Others	ADP	0.0	-20.0	-35.0	-32.0	0.0	-10.0	-24.0	-26.0
	Formate	0.0	-28.0	-38.0	-41.0	n.d.	n.d.	n.d.	n.d.
	2-Oxoisocaproate	0.0	6.0	70.0	72.0	n.d.	n.d.	n.d.	n.d.

(b)

Incubation time (h)		24				48			
Molar concentration (μM)		0	50	75	100	0	25	50	100
Glycolysis	α-GLC §	0.0	-6.0	-12.0	-22.0	0.0	-18.0	-16.0	-24.0
	Lactate	0.0	-28.0	-57.0	-71.0	0.0	-46.0	-65.0	-85.0
	Succniate	0.0	10.0	14.0	9.0	n.d.	n.d.	n.d.	n.d.
	AcOH	0.0	12.0	46.0	96.0	0.0	60.0	103.0	170.0
	Leucine §	0.0	10.0	9.0	20.0	0.0	6.0	10.0	31.0
	Isoleucine §	n.d.	n.d.	n.d.	n.d.	0.0	6.0	10.0	35.0
Amino acids metabolism	Phenylalanine §	n.d.	n.d.	n.d.	n.d.	0.0	2.0	15.0	26.0
	Methionine §	n.d.	n.d.	n.d.	n.d.	0.0	4.0	8.0	28.0
	Alanine	0.0	9.0	-12.0	-21.0	n.d.	n.d.	n.d.	n.d.
Ketone body biosynthesis	Acetone	0.0	43.0	142.0	239.0	0.0	13.0	37.0	93.0
Glutathione biosynthesis	Pyroglutamate	0.0	4.0	-10.0	-12.0	n.d.	n.d.	n.d.	n.d.
Phospholipid metabolism	Choline	n.d.	n.d.	n.d.	n.d.	0.0	-22.0	-10.0	-50.0
	Propylene Glycol	0.0	-11.0	-14.0	-24.0	0.0	-20.0	-28.0	-58.0
Others	Formate	0.0	-21.0	-34.0	-45.0	0.0	-30.0	-45.0	-41.0
	3-Methyl-2-oxovalerate	n.d.	n.d.	n.d.	n.d.	0.0	-13.0	-14.0	-32.0

% shift
- -100
- -75
- -50
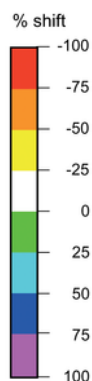- -25
- 0
- 25
- 50
- 75
- 100

Figure 7

Summary of statistical data analysis through heatmaps scheme to demonstrate the percentage increase and decrease of selected metabolites levels calculated considering the control sample levels as reference. In (a) are listed the results for the endometabolome of cell extracts and in (b) for the exometabolome of culture media samples addressing FN1 cells treated as a function of dose and incubation time with AgNP and the metabolic pathways where they can play a role. Numeric values were also provided to estimate

the magnitude of the shifts. Consecutive colors were surrounded by solid black lines when the levels were statistically different by Fisher's pairing method (separated groups, $p < 0.05$). Keys: Symbol "§" is used to single out those exometabolites present initially in the media culture and therefore consumed by cells, and "n.d." stands for non-detectable as a group classifier.

(a)

Incubation time (h)		24				48			
Molar concentration (μM)		0	50	75	100	0	25	50	100
Glycolysis	Lactate	0.0	-16.0	-35.0	-29.0	n.d.	n.d.	n.d.	n.d.
	AcOH	0.0	33.0	63.0	166.0	0.0	16.0	25.0	63.0
Amino acids metabolism	Alanine	0.0	-32.0	-64.0	-62.0	0.0	-9.0	-41.0	-54.0
	Glycine	0.0	-21.0	-43.0	-57.0	0.0	-8.0	-8.0	-28.0
	Leucine	0.0	7.0	17.0	20.0	0.0	-2.0	-12.0	-14.0
	Isoleucine	n.d.	n.d.	n.d.	n.d.	0.0	-1.0	-21.0	-33.0
Energy source	Creatine	0.0	-53.0	-73.0	-91.0	0.0	-24.0	-46.0	-77.0
Phospholipid metabolism	O-Phosphocholine	0.0	-57.0	-70.0	-91.0	n.d.	n.d.	n.d.	n.d.
	Sn-Glycero-3-PC	0.0	-24.0	-28.0	-67.0	0.0	-15.0	-45.0	-70.0
Antioxidant agent	NADP$^+$	0.0	-25.0	-26.0	-31.0	0.0	-3.0	-15.0	-37.0
	N-Acetylcysteine	0.0	-3.0	-30.0	-67.0	0.0	-29.0	-61.0	-91.0
Others	UDP-GlcNAc	0.0	-54.0	-28.0	-69.0	0.0	-23.0	-61.0	-85.0
	Valerate	0.0	3.0	58.0	75.0	0.0	4.0	14.0	19.0
	AMP	0.0	-1.0	-34.0	-48.0	n.d.	n.d.	n.d.	n.d.

(b)

Incubation time (h)		24				48			
Molar concentration (μM)		0	50	75	100	0	25	50	100
Glycolysis	α-GLC §	0.0	-9.0	-10.0	-29.0	0.0	-15.0	-24.0	-45.0
	Lactate	0.0	-31.0	-56.0	-74.0	0.0	-30.0	-31.0	-61.0
	AcOH	0.0	119.0	162.0	161.0	0.0	77.0	104.0	134.0
Amino acids metabolism	Leucine§	0.0	32.0	57.0	82.0	0.0	5.0	35.0	36.0
	Isoleucine §	0.0	n.d.	n.d.	n.d.	0.0	25.0	46.0	47.0
	Alanine	0.0	-13.0	-18.0	-40.0	n.d.	n.d.	n.d.	n.d.
Ketone body biosynthesis	Acetone	0.0	27.0	166.0	173.0	0.0	5.0	49.0	79.0
Glutathione biosynthesis	Pyroglutamate	0.0	-12.0	-20.0	-41.0	0.0	-19.0	-39.0	-46.0
Others	N-Acetylglutamate	0.0	37.0	39.0	58.0	0.0	11.0	31.0	30.0
	N-Acetylaspartate	0.0	15.0	11.0	29.0	0.0	12.0	65.0	69.0
	Propylene Glycol	0.0	-20.0	-45.0	-60.0	0.0	-10.0	-71.0	-66.0
	Cadaverine	0.0	-12.0	-33.0	-28.0	0.0	-5.0	-20.0	-33.0
	Formate	0.0	-22.0	-41.0	-64.0	0.0	-7.0	-41.0	-58.0

% shift

	-100
	-75
	-50
	-25
	0
	25
	50
	75
	100

Figure 8

Summary of statistical data analysis through heatmaps scheme to demonstrate the percentage increase and decrease of selected metabolites levels calculated considering the control sample level as reference. In (a) are shown the results for the endometabolome of cell extracts and in (b) for the exometabolome of culture media samples addressing HUV-EC-C cells treated as a function of dose and incubation time with AgNP and the metabolic pathways where they can play a role. Numeric values were also provided to estimate the magnitude of the shifts. According to Fisher's pairing method, consecutive colors were surrounded by solid black lines when the levels were statistically different (separated groups, $p < 0.05$). <u>Keys</u>: Symbol "§" is used to single out those exometabolites present initially in the media culture and therefore consumed by cells, and "n.d." stands for non-detectable as a group classifier.
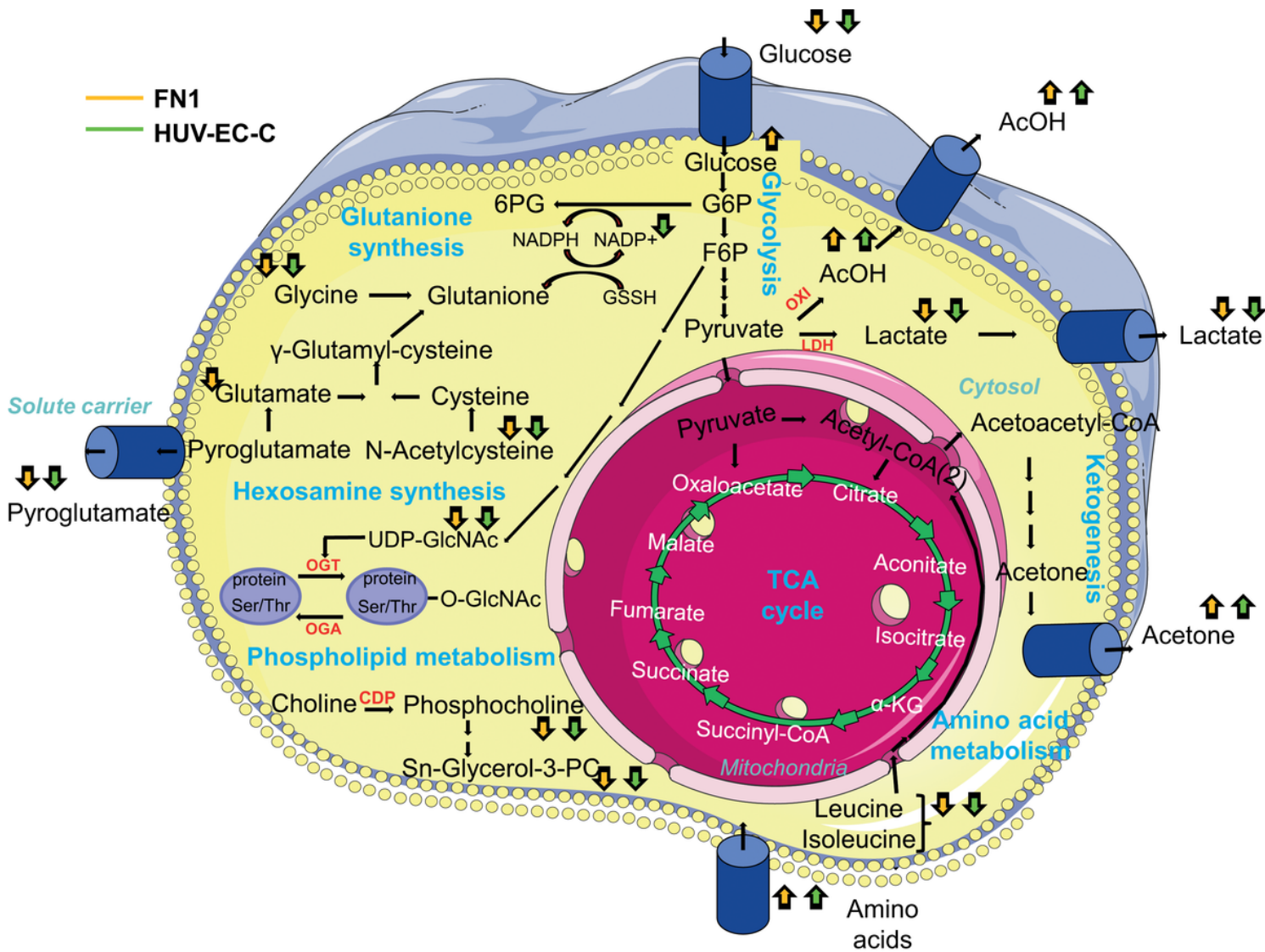

Figure 9

Summary of identified metabolic pathways that are changing with dose and time dependent silver treatments showing tendencies of increase/decrease the metabolites levels as informed in Fig. 7 and Fig. 8. Brown arrows are ascribed to cells from FN1 lineage while green arrows are ascribed to cells from HUV-EC-C lineage. <u>Abbreviations</u>: OGT for O-GlcNAc transferase, OGA for OGlcNAcase, CDP for Cytidine 5'-

diphosphocholine, G6P for Glucose 6-phosphate, F6P for Fructose 6-phosphate, TCA for Tricarboxylic acid cycle, OXI for oxidation, and LDH for Lactate dehydrogenase. Figure adapted from "Servier Medical ART," a repository of free medical images provided by Les Laboratoires Servier (http://smart.servier.com) and licensed under a Creative Commons Attribution 3.0 Unported License.

Supplementary Files

This is a list of supplementary files associated with this preprint. Click to download.

- SupplementaryInformation.docx